

Fast ion confinement and stability in a neutral beam injected reversed field pinch

J. K. Anderson, A. F. Almagri, D. J. Den Hartog, S. Eilerman, C. B. Forest et al.

Citation: *Phys. Plasmas* **20**, 056102 (2013); doi: 10.1063/1.4801749

View online: <http://dx.doi.org/10.1063/1.4801749>

View Table of Contents: <http://pop.aip.org/resource/1/PHPAEN/v20/i5>

Published by the [American Institute of Physics](#).

Additional information on Phys. Plasmas

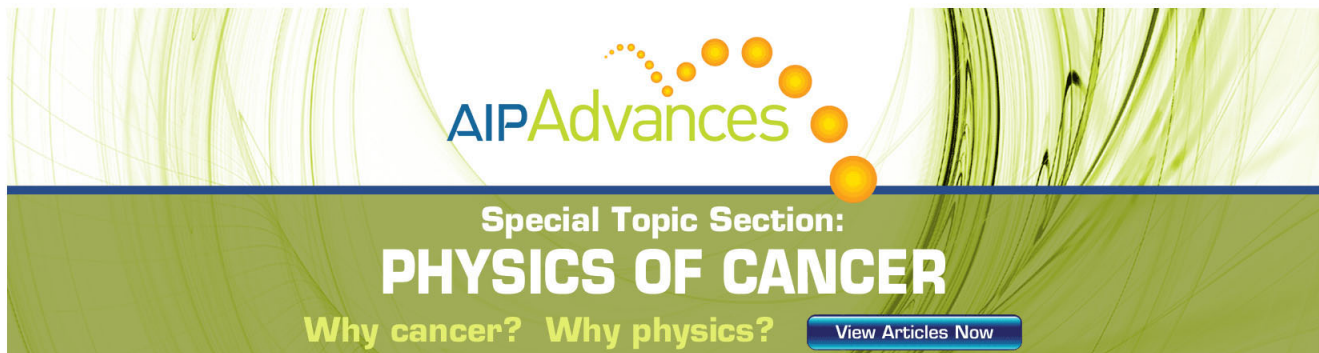
Journal Homepage: <http://pop.aip.org/>

Journal Information: http://pop.aip.org/about/about_the_journal

Top downloads: http://pop.aip.org/features/most_downloaded

Information for Authors: <http://pop.aip.org/authors>

ADVERTISEMENT



AIPAdvances

Special Topic Section:
PHYSICS OF CANCER

Why cancer? Why physics? [View Articles Now](#)

Fast ion confinement and stability in a neutral beam injected reversed field pinch^{a)}

J. K. Anderson,^{1,b)} A. F. Almagri,¹ D. J. Den Hartog,¹ S. Eilerman,¹ C. B. Forest,¹
 J. J. Kollner,¹ V. V. Mirnov,¹ L. A. Morton,¹ M. D. Nornberg,¹ E. Parke,¹ J. A. Reusch,¹
 J. S. Sarff,¹ J. Waksman,¹ V. Belykh,² V. I. Davydenko,² A. A. Ivanov,² S. V. Polosatkin,²
 Y. A. Tsidulko,² L. Lin,³ D. Liu,⁴ G. Fiksel,⁵ H. Sakakita,⁶ D. A. Spong,⁷ and J. Titus⁸

¹University of Wisconsin, Madison, Wisconsin 53706, USA

²Budker Institute of Nuclear Physics, Novosibirsk, Russia

³University of California, Los Angeles, California 90095, USA

⁴University of California, Irvine, California 92697, USA

⁵Laboratory for Laser Energetics, Rochester, New York 14623, USA

⁶National Institute of Advanced Industrial Science and Technology, Tsukuba, Japan

⁷Oak Ridge National Laboratory, Oak Ridge, Tennessee 37831, USA

⁸Florida Agricultural and Mechanical University, Tallahassee, Florida 32307, USA

(Received 16 November 2012; accepted 3 February 2013; published online 15 April 2013)

The behavior of energetic ions is fundamentally important in the study of fusion plasmas. While well-studied in tokamak, spherical torus, and stellarator plasmas, relatively little is known in reversed field pinch plasmas about the dynamics of fast ions and the effects they cause as a large population. These studies are now underway in the Madison Symmetric Torus with an intense 25 keV, 1 MW hydrogen neutral beam injector (NBI). Measurements of the time-resolved fast ion distribution via a high energy neutral particle analyzer, as well as beam-target neutron flux (when NBI fuel is doped with 3–5% D₂) both demonstrate that at low concentration the fast ion population is consistent with classical slowing of the fast ions, negligible cross-field transport, and charge exchange as the dominant ion loss mechanism. A significant population of fast ions develops; simulations predict a super-Alfvénic ion density of up to 25% of the electron density with both a significant velocity space gradient and a sharp radial density gradient. There are several effects on the background plasma including enhanced toroidal rotation, electron heating, and an altered current density profile. The abundant fast particles affect the plasma stability. Fast ions at the island of the core-most resonant tearing mode have a stabilizing effect, and up to 60% reduction in the magnetic fluctuation amplitude is observed during NBI. The sharp reduction in amplitude, however, has little effect on the underlying magnetic island structure. Simultaneously, beam driven instabilities are observed as repetitive $\sim 50 \mu\text{s}$ bursts which coincide with fast particle redistribution; data indicate a saturated core fast ion density well below purely classical predictions. © 2013 AIP Publishing LLC [<http://dx.doi.org/10.1063/1.4801749>]

INTRODUCTION

The envisioned burning plasma experiment, regardless of magnetic concept, relies on sufficient confinement of the charged fusion product for plasma self heating. As such, the confinement of fast ions and their impact on the bulk plasma are crucial issues.

A tremendous body of work demonstrates that fast ions in a tokamak plasma (born from fusion reactions, ICRF, or NBI) are generally well confined and thermalize via classical Coulomb collisions. However, a sufficiently intense fast ion population can excite collective instabilities that can lead to resonant fast ion transport.¹

A new body of work on the effects of a large fast ion population in the reversed field pinch (RFP) configuration has recently been opened. Despite the RFP's weak toroidal field and multiple resonant tearing modes which could diminish fast ion confinement,^{2,3} NBI-born fast ions in low

concentration are observed to slow classically and have a confinement time much larger than thermal particles.⁴ The dearth of transport within the modestly stochastic magnetic field is understood to result from the decoupling of the fast ion orbits from the magnetic perturbations. The ions are routinely confined for up to a classical slowing time.⁵

In this work, we investigate the effect of a large NBI-generated fast ion density on plasma stability in the RFP and the resulting effect of altered stability on the fast ion confinement. There are two observations regarding stability in the NBI-heated RFP, one each of a stabilizing and destabilizing phenomenon. First, the core-most tearing mode undergoes a substantial reduction in amplitude during NBI. It turns out, somewhat surprisingly, that the sharp reduction in mode amplitude has little effect on the underlying magnetic island structure due to a subtle coincident equilibrium change. There is no measurable effect on fast ion confinement and only a modest (at most) effect on the thermal confinement.

Conversely, at high fast ion densities, the onset of beam-driven instabilities has a strong adverse effect on the

^{a)}Paper JI2 4, Bull. Am. Phys. Soc. **57**, 151 (2012).

^{b)}Invited speaker. Electronic mail: jkanders@wisc.edu.

confinement of the fast particles. In a set of well-studied discharges, TRANSP⁶ predicts both a steep velocity gradient and spatial gradient in the fast ion density with n_{fi} as high as 25% of n_e . Repetitive bursts of 50–200 kHz magnetic activity ($\leq 100 \mu\text{s}$ duration) comprised of both an EPM-like $n=5$ and an Alfvénic $n=4$ mode spontaneously occur.⁷ Nonlinear coupling between the modes coincides with redistribution of core-localized fast ions.⁸ Data from an experimental scan of beam power indicate a saturated core fast ion density well below the TRANSP prediction.

In a different class of discharge, where a reduced core electron temperature leads to rapid slowing of the beam-born ions, the measured velocity gradient is much smaller. In these discharges, a comparatively long-lived (up to 1 ms) chirping beam-driven mode is observed whose frequency can decrease by a factor of two or more.

THE RFP AS A TEST BED FOR FAST ION PHYSICS

The RFP presents unique opportunities for the studies of fast ion physics, as it is characterized by a very high current density (relative to toroidal magnetic field strength), and nearly all the confining field is generated by current within the plasma. The toroidal field is weak—of the same order as the poloidal field—as illustrated in Fig. 1(a); a typical

Madison Symmetric Torus (MST) discharge studied in this work has total toroidal plasma current of 300 kA, a core $B_\phi \sim 0.3 \text{ T}$, and a poloidal magnetic field that reaches a maximum of about 0.2 T at mid-radius. The modulus of the magnetic field takes on a profile very different than that found in the tokamak: the field is strongest at the magnetic axis, and as the poloidal magnetic field is dominant beyond mid-radius, $|B|$ on a poloidal flux surface near the edge undergoes only about a 10% variation from outboard to inboard side of the machine. In contrast, a particle on an edge flux surface in a tokamak experiences a very large change in field strength moving from the outboard to inboard midplane. This distinction has an effect on the particle orbits and trapped fraction of fast ions. The resulting q profile (see examples in Fig. 6(a)) is strongly sheared, implying strong damping of modes in the Alfvén continuum and has many rational surfaces where long wavelength $m=1, n \geq 5$ tearing modes are resonant. A substantial overlap of magnetic islands can occur and as such, the magnetic field in the RFP is typically stochastic. Indeed, thermal confinement in the standard RFP is governed by Rechester-Rosenbluth-like transport.⁹ Nested magnetic surfaces can be restored in two known ways. The first technique substantially reduces tearing mode amplitudes by modification of the current profile and leads to an axisymmetric configuration with tokamak-like bulk confinement.¹⁰ The second technique is a transition to a single helicity state: the amplitude of the core-most magnetic mode grows rapidly as the amplitudes of secondary modes are suppressed.¹¹ This so-called Single Helicity Axis state (SHAx) has a helical (as opposed to axisymmetric) core, surrounded by good magnetic surfaces and is often accompanied by an improved confinement state.¹²

A neutral beam injector optimized for MST is now routinely used to study fast ion physics in the RFP. The MST¹³ ($R/a = 1.5 \text{ m}/0.52 \text{ m}$) operates with a plasma current between 200 and 600 kA, a line averaged electron and deuteron density typically less than $2 \times 10^{13} \text{ cm}^{-3}$ and a core electron temperature of 200–2000 eV. The NBI operates at accelerating energy 25 keV with up to 1 MW of neutral power delivered to the plasma for a pulse of up to 20 ms—a sufficient duration as it is a substantial fraction of the MST pulse, several times the typical τ_e, τ_p of thermal particles and on the order of the classical slowing time for the discharges of primary interest in this work. The beam is compact, as shown in the scale drawing Fig. 1(b), which also illustrates the tangential trajectory of the incident neutrals. The radius of tangency is $R = 1.41 \text{ m}$, slightly inboard of the magnetic axis. The beam is geometrically focused for accessing the MST plasma through an 11 cm diameter port (kept small as it is important to minimize disturbances in the close-fitting conducting shell on the MST) and boasts a high full energy component of around 86%. The beam fuel is mainly hydrogen with a small fraction (3%–5%) of deuterium for monitoring fast ion content via beam-target fusion neutrons; beam operation adds only a negligible amount of fuel to the MST discharge. For the typical discharges studied in this work, the fast hydrogen particles are slightly super-Alfvénic ($v_{\parallel,H} \approx 1.25 v_A$) and have substantial Larmor radii $\rho_f \approx .04 \text{ m}$ or $\rho_f/a \approx 0.1$.

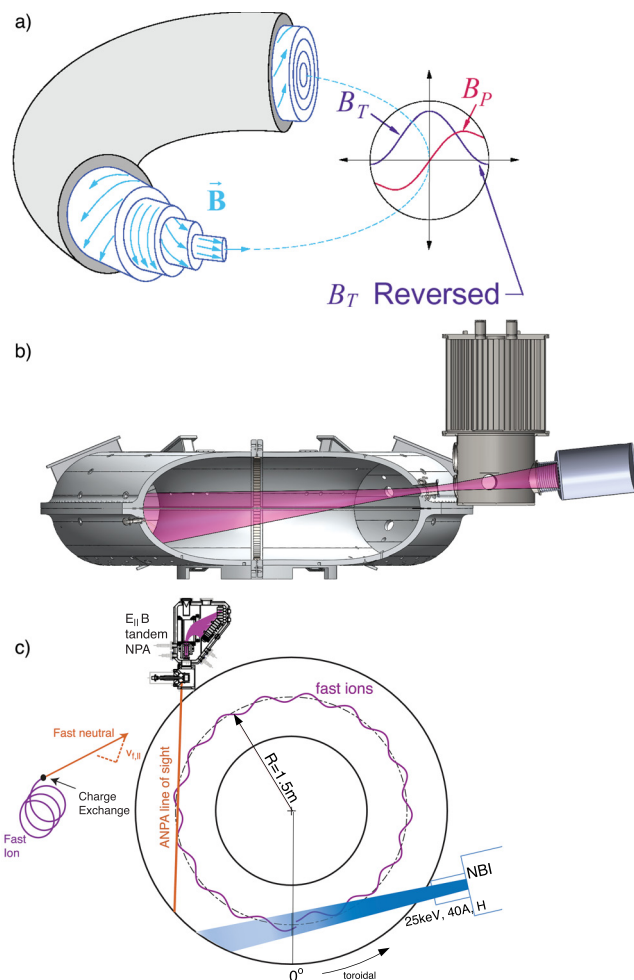


FIG. 1. (a) Magnetic surfaces and profiles in the RFP, (b) a scale drawing of the 25 keV, 1 MW tangential NBI on MST, (c) a top view of MST indicating the relative location of the NBI and neutral particle analyzer.

The key diagnostics in this work measure edge and internal magnetic fluctuations, and the fast particle content by neutral particle analysis and a fusion neutron detector. A toroidally distributed array of 64 Mirnov coils located on the inside surface of the MST vessel, just outside the last closed flux surface, measures the toroidal and poloidal components of boundary field fluctuations. Tearing modes are the most prevalent perturbations, measured between 10 and 30 kHz, while higher frequency activity (50–300 kHz) is measurable during NBI. Edge magnetics correlate with core localized magnetic perturbations measured with a FIR polarimeter.¹⁴ A high energy advanced neutral particle analyzer (ANPA)¹⁵ is located on a tangential viewing chord and measures a convolution of core-localized high pitch ions and mid-radius-to-edge fast ions with higher v_{\perp} due to line-of-sight considerations.¹⁶ Figure 1(c) is a top view of the MST showing the relative position of the NBI and the ANPA; the line of sight does not intersect the neutral beam and as such the measured signal is provided by passive charge exchange. The energy resolution is about 3 keV per channel and the range extends beyond the beam injection energy.¹⁷ A typical measurement of the NBI-generated fast ion dynamics is in Fig. 2. This class of discharges, with plasma current of 300 kA and a magnetic boundary condition of $q(a) = 0$, is referred to several times in the analyses below. In Fig. 2(a), the plasma current and neutral beam injection pulse are plotted. The small concentration of deuterium in the beam fuel leads to a measurable beam-target neutron flux during (and after) NBI (Fig. 2(b)). The measured fast ion distribution (by neutral particle analysis) is depicted in the color contour plot (Fig. 2(c)) with logarithmic color scale. The fast ion content is extracted from the measured NPA signal by normalizing by the time varying neutral density level, as measured by an array of D_{α} detectors. There is a clear peak in the energy distribution at the injected 25 keV, and a second faint peak near the half-energy component. The fast ion population develops quickly, reaching its maximum within a few ms following the start of NBI, and the particles slow classically following the end of the NBI pulse. Figures 2(d) and 2(e) are typical electron density and temperature profiles, measured at 26 ms into the discharge. Coupled with the TRANSP prediction of core-localized, high pitch fast ions (Fig. 4), estimates of the background neutral density profile, and computations of particle re-ionization along the ANPA line of sight, it is deduced that the ANPA is primarily sampling core-localized high pitch ions. While not absolutely calibrated, the ANPA measurement is an oft-utilized qualitative indicator of the core localized, high pitch fast particle content.

CONFINEMENT OF BEAM-INJECTED FAST IONS IN THE RFP

The confinement of fast ions is relatively insensitive to the stochastic field of the RFP. This is understood through computation of fast particle orbits within the turbulent field and inspection of guiding center islands, which differ significantly from magnetic islands.⁵ The fast ion energy loss rate is consistent with classical slowing (time scale typically

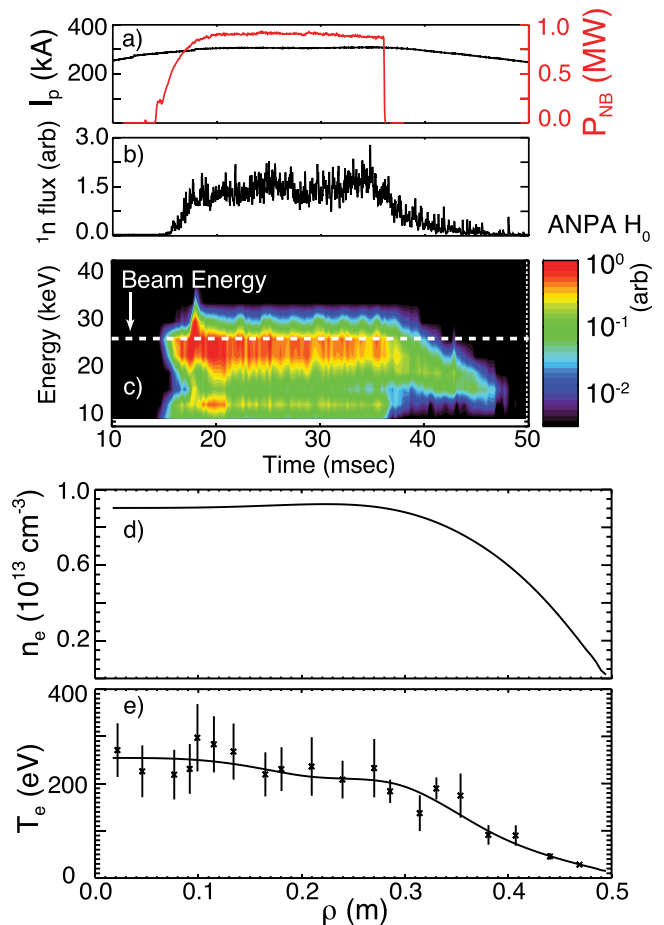


FIG. 2. Example of the measured fast ion dynamics during NBI. (a) The time trace of a typical 300 kA plasma current discharge with timing of the neutral beam injection. (b) The neutron flux is an indicator of the volume-averaged fast particle content (of the small fraction of deuterium beam fuel), while panel (c) is a color contour depiction of the measured core-localized parallel fast hydrogen distribution, by normalizing the NPA signals by background neutral density strength versus time. Panels (d) and (e) are typical radial electron density and temperature profiles as measured at 26 ms into the discharge.

20 ms) and the fast ion particle confinement time is much larger than that of thermal particles.

The decay of neutron flux after turn-off of a short beam pulse (the beam-blip technique¹⁸), is used to infer the confinement of the fast particles, τ_{fi} . The details of the τ_{fi} measurement over a range of stochasticity (and hence collisionality, by the strong effect on electron temperature) is presented in Ref. 4. It is important to note that the beam blip technique keeps the total fast ion content small, and the possible effects of a large fast ion population are not important. Over a large range of MST operating space, the confinement of fast particles is much better than thermal, and (within the sizable error bars of a neutral density measurement) consistent with charge exchange as the primary loss mechanism. In standard-stochasticity level discharges, the electron energy and particle confinement is of order 1 ms, while the fast ion particle confinement can be 10–20 ms. The trend continues into the low stochasticity axisymmetric limit, where thermal confinement times can increase to 5–10 ms and the fast ion confinement time is routinely greater than 30 ms.

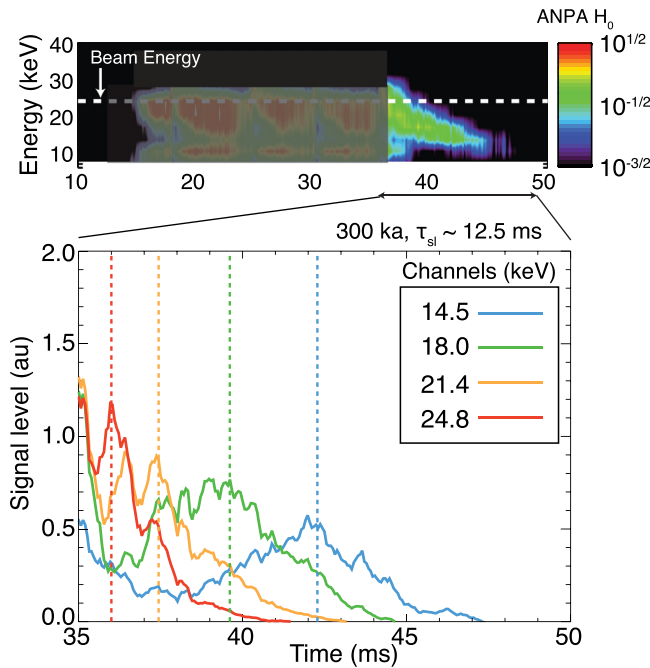


FIG. 3. Expanded view of fast hydrogen behavior following beam turn-off. With zero source, the fast hydrogen particles slow classically as the vertical dashed lines are the expected times of peak signals in each of the next four lower energy channels for classical slowing at $\tau_{sl} = 12.5$ ms.

Figure 3 is a demonstration of the classical slowing of fast hydrogen particles within the plasma. The measured distribution during NB injection is shaded to guide the eye to the 15 ms following beam turn-off. The signal from each of the four highest energy channels is plotted versus time in the expanded view. At the time that the source is turned off, there is an abundance of particles at the beam injection energy; for well-confined particles, there is an expected shift in peak signal to successively lower energy channels. The vertical dashed lines indicate timing of peaks in each of the next four lower energy channels expected for classical slowing at a $\tau_{sl} = 12.5$ ms, taking into account the finite energy width and response of the NPA. There is clear agreement with the timing of the measured signals.

While the measurements are consistent with energy loss times predicted by classical slowing alone, it is difficult to compute a fast particle confinement time in this analysis.

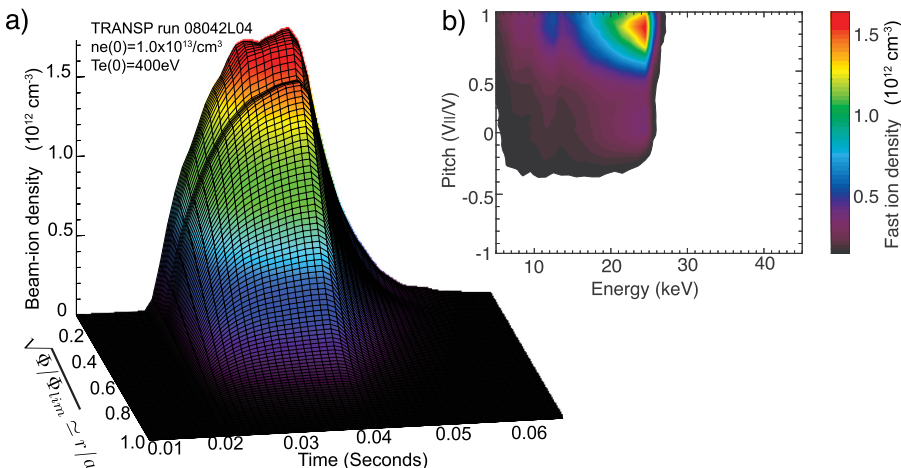


FIG. 4. TRANSP prediction of fast ion distribution in MST. In plot (a), the fast ion density in MST is core-peaked and ramps up for the 20 ms injection. Plot (b) shows the predicted distribution midway through the beam injection period; the ions are predominantly high pitch and peaked near the beam injection energy.

The TRANSP-modeled fast ion population is core-localized with a high pitch ($v_{\parallel}/|v|$). A typical example of TRANSP output for an MST discharge with line average electron density of about $1 \times 10^{13} \text{ cm}^{-3}$ is in Fig. 4. Figure 4(a) is a plot of the fast particle density versus time and radius; the velocity-integrated fast ion density ramps up for the 20 ms duration of the injection and is maximum in the core. TRANSP routinely predicts a peak $n_{fi}/n_e \sim 0.15$ and for certain conditions can predict $n_{fi}/n_e \sim 0.25$. Figure 4(b) is a contour plot of the fast ion distribution versus energy and pitch at a single time slice midway through beam injection, demonstrating the fast ions are strongly aligned with the magnetic field ($v_{\parallel}/|v| \geq 0.8$) and the predominantly passing particles are above the Alfvén speed of the background plasma, with a typical $v_{\parallel,H} \approx 1.25v_A$.

EFFECTS OF A LARGE FAST ION POPULATION IN THE RFP

As the beam-born particles are much better confined than the bulk, a substantial population of fast ions develops during NBI and affects the background plasma in several ways. There is a strong toroidal torque applied to the plasma and an accompanying strong effect on the rotation. In the low stochasticity limit (when the thermal energy confinement time becomes a significant fraction of the fast ion energy slowing time), there is an expected and observed modest heating of the bulk plasma.¹⁹ There is also a measurable change to the equilibrium current density profile, consistent in direction with a small parallel beam-driven current, but the interpretation is complicated by simultaneous changes to core localized magnetic fluctuations which may suppress inductively driven current. The fast ions have both a stabilizing and destabilizing effect on the plasma.

Suppression of core tearing mode by NBI

The core-most tearing mode is suppressed by NBI over a wide range of equilibria in MST. Figure 5 is a particularly clean example of the core mode suppression. Here, several discharges with and without NBI are averaged to reduce statistical noise. In this case of lower plasma current, $I_p = 200$ kA (Fig. 5(a)), and a line-averaged density of about $0.7 \times 10^{13} \text{ cm}^{-3}$ (Fig. 5(b)), the $n = 5$ tearing mode is

resonant near the core as $q(0) \geq 0.2$. Its amplitude is plotted with and without NBI in Fig. 5(c), and a suppression factor is defined in Fig. 5(d) as the change in edge-measured fluctuation amplitude normalized to the non-NBI discharge value, around 60% in this example.

While the core-most mode is strongly suppressed, the outer modes are relatively unaffected. Figure 6(a) shows q profiles from two distinct MST equilibria. Plotted in red is the q profile from a $q(a)=0$ discharge; a second q profile from a deeply reversed discharge is plotted in blue. In the case of $q(a)=0$, the mode suppression factor is plotted in red for each resonant toroidal mode number $5 \leq n \leq 15$ in Fig. 6(b). For the deeply reversed case, the $n=5$ mode is not resonant—a maximum value of $q(0)$ is less than the requisite $1/5$ —placing the $n=6$ mode closest to the plasma core. The mode suppression factors for the $6 \leq n \leq 15$ modes in the deeply reversed discharge are plotted in blue. In both cases, the core-most resonant mode is strongly suppressed by NBI, while the modes resonant at larger radii are unaffected: the suppression factor uncertainty (a computed standard deviation over the averaging window) overlaps zero for all secondary modes. Limited experiments with neutral beam counter-injection into 300 kA discharges have been performed with no measurable effect on tearing mode amplitudes, however, counter-injected fast ions are not as well confined in MST.⁴ Tearing suppression relies on a large population of fast ions at the mode resonant surface; the fast ions again are apparently core localized.

Stabilization (albeit partial) of the tearing modes should come as no surprise, as there are many observations of fast ions having a stabilizing influence on sawteeth in tokamaks (see Ref. 20 and references therein). The physical picture of circulating (as opposed to trapped) fast ions suppressing tearing modes²¹ is quite applicable here, and the differing effects

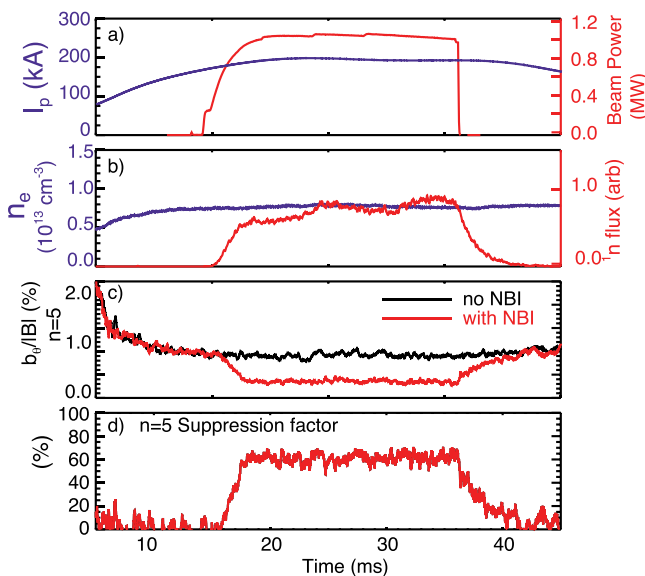


FIG. 5. NBI-induced suppression of the core-most ($n=5$ in this case) tearing mode. Panel (a) is the plasma current and NB injection versus time, (b) is the line-averaged electron density and neutron flux versus time, and panel (c) is the measure of the magnetic fluctuation amplitude of the core-most tearing mode with and without NBI. Also defined (d) is the mode suppression factor, used as a proxy of core fast ion content.

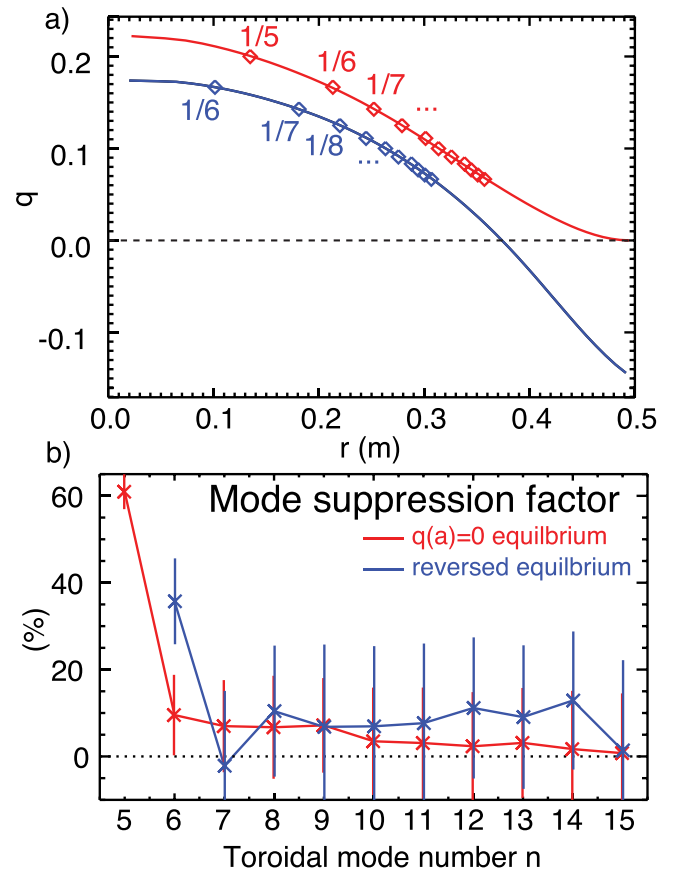


FIG. 6. For two distinct equilibria, the NBI has a stabilizing influence on the core-most tearing mode while the secondary modes are unaffected. In these two examples, q profiles plotted in (a) are separated by a strong variation in the $q(a)$ boundary condition. Reduction of the core-most resonant modes (b) is observed at different toroidal mode numbers, n in each case; modes resonant at larger radii are unaffected.

on tearing of co- versus counter-injected fast ions have been investigated.²² Work has also been conducted specifically for the RFP where finite Larmor radius effects are more pronounced,²³ more recent analytical work points to a gradient in fast ion density playing a key role.²⁴

In pursuit of systematic study of the fast ion confinement in the RFP, we investigate the possible feedback of reduced core tearing activity on the confinement of the fast ions. Earlier results⁵ show that confinement is only weakly affected by standard levels of stochasticity, which suggests the effect will be weak. This in fact turns out to be true, but with a somewhat surprising result: due to a coincident change in the equilibrium, the strong reduction of the core mode amplitude has very little effect on the island width and overall stochasticity. The NB-injected discharges experience a small but measurable peaking in the parallel current density profile, and the on-axis value of the safety factor drops as shown in Fig. 7. Equilibrium reconstructions of both NBI and non-NBI 300 kA discharges with boundary value of $q(a)=0$ show the change in q profile. The black curve is the q profile of the non-NBI discharge, while the NB injected case is shown in red. Each analysis was performed at a time near $t=25$ ms; there is a substantial uncertainty in the actual value of q at the core, but the subtle motion of the $q=1/5$ surface is confirmed by fluctuation analysis of Ampere's law

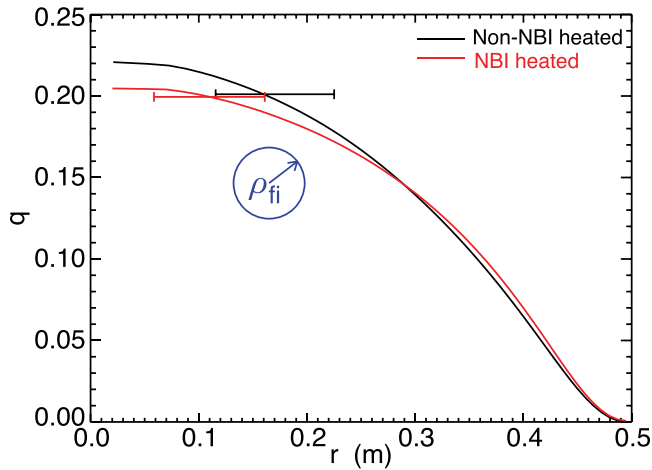


FIG. 7. q profiles of NBI (red) and non-NBI (black) discharges at 300 kA and $q(a)=0$. The island width for each case is included (offset minimally from 0.2 in each curve for clarity). Also plotted is a typical fast ion gyroradius (blue) for a 25 keV $v_{||}/|v| = 0.8$ fast hydrogen ion, indicating the gyro motion is of the same length scale as the island width.

using a multi-chord polarimeter. The magnetic field perturbation associated with the $n=5$ tearing mode clearly moves radially inward through the line of sight of one of the vertically-viewing chords. This places the resonant surface in a region with lower magnetic shear. The island width of the $m=1$ mode is calculated²⁵ as $w = 4\sqrt{\frac{\tilde{b}_r r}{B_0 n q}}$, and even considering a 50% reduction in mode amplitude, the island width is not significantly altered. These widths are included for both cases in Fig. 7.

The slight inward shift of the $q=1/5$ surface does not alter the underlying stochasticity of the plasma, as the Rechester-Rosenbluth-defined island overlap parameter remains well into the stochastic regime.²⁶ No observable change in fast ion or thermal confinement results from the suppression of only the core-most tearing mode.

Beam driven instabilities

Recently published work⁷ reports multiple beam driven instabilities in 300 kA $q(a)=0$ discharges described above. In these discharges, with a strong measured velocity gradient in fast ion distribution (Fig. 2), there are a pair of modes that occur in coincident bursts (of about $50 \mu\text{s}$ duration). An EPM-like $n=5$ mode is immediately followed by an $n=4$ Alfvénic mode. The categorization of the bursting magnetic activity is made by monitoring the mode frequency with a scan of fast ion speed (by NBI energy) and by scanning the bulk Alfvén speed (by varying the density, majority ion mass and magnetic field strength). These studies show the precursory $n=5$ mode frequency is proportional to the speed of the fast ions, and the frequency of the $n=4$ mode is strongly related to the bulk Alfvén speed. The measured frequency of the Alfvénic mode is below the predicted TAE gap, and it is a matter of ongoing computation to determine if the modes are excited in a different gap (e.g., BAE or BAAE), or are strongly driven continuum modes.

The internal magnetic mode structure of the bursting EPM-like mode has been measured by FIR polarimetry. In a

related analysis, nonlinear coupling between the EPM-like and AE-like modes is observed, including an appropriate wavenumber and frequency addition rule and strong bicoherence. Additionally, the coupling between the beam driven modes coincides with fast particle redistribution: a significant drop in the NPA measurement of core-localized 25 keV hydrogen ions is apparent with a fast analysis. Hundreds of similar bursts are averaged together to obtain a sufficient signal-to-noise ratio at time resolution of $10 \mu\text{s}$.⁸ These results are consistent with the previously discovered physics in other devices as reported, for example, in Refs. 27–29.

While MST is well diagnosed for measurements of fast internal fluctuations, the fast ion and fast ion loss diagnostics are currently limited. However, an experimental knob that has proven quite useful with the available diagnostics is a scan of the injected neutral beam power. In the analysis shown in Fig. 8, two sets of discharges are averaged together to expose the effect of beam power. In red, the beam power (Fig. 8(a)), neutron flux (Fig. 8(d)), core ANPA full energy channel (Fig. 8(e)), and $n=5$ tearing mode suppression factor (Fig. 8(f)) are plotted for full beam power, and their reduced-power counterparts are plotted in green. Additionally, a spectrogram of the beam-driven instability is plotted for each case (Figs. 8(b) and 8(c)). The spectrograms clearly show a delayed onset of the beam-driven mode at reduced power, consistent with a finite fast ion accumulation time. The discharges appear to reach a saturated fast hydrogen density at less than full beam power and increased NB power strongly enhances the beam-

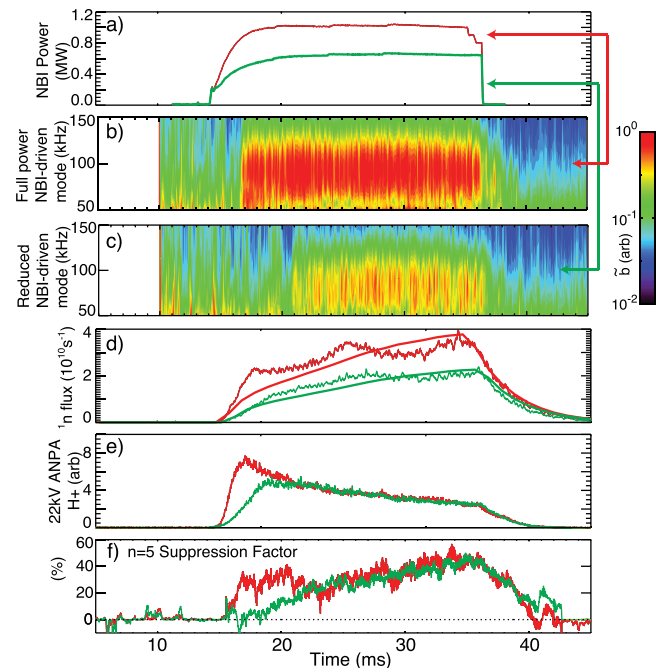


FIG. 8. Two ensembles of discharges with full beam power (1 MW red) and reduced beam power, (0.6 MW green). In panel (a), the two different beam injection conditions are plotted versus time. The high frequency magnetic activity associated with beam-driven instabilities are plotted for the 1 MW injection case (b), and the reduced power case (c). Panel (d) is the fusion neutron flux (a proxy for the volume averaged fast deuterium content) versus time for the two cases; while panel (e) is the ANPA measure of core-localized, high pitch fast hydrogen particles. A measure of the fast-ion induced suppression of the core-most tearing mode is plotted for each case in panel (f).

driven mode, similar to observations in some tokamak discharges.³⁰ Noting that the beam fuel is mostly hydrogen with about 5% deuterium, the neutron flux for each case (plotted in the fourth panel) is indicative of a small concentration of fast particles (up to about 1% of the core electron density), while TRANSP would predict a fast hydrogen density approaching 20% of $n_e(0)$. The 22 kV ANPA signal is a measure of the core-localized, parallel, full energy fast hydrogen content, and the difference in the time dependence of these pairs of signals provide evidence of significantly different behavior. The neutron flux in each case, following an initial rapid rise, continues to rise slowly and attain a value proportional to the source (beam power). While the neutron detector currently lacks an absolute calibration, applying a single factor to the measurement can make both curves match TRANSP predictions (plotted as solid lines) except for some subtle time dependence. The ANPA signals lead to a very different conclusion on fast hydrogen content, as the signals for both source rates asymptote to the same value, while classical considerations alone (e.g., TRANSP) predict a ratio equal to the ratio of particle source. The lower power case follows a longer timescale to reach saturation. In Fig. (8(f)), the $n = 5$ mode suppression factor is plotted for each case. Again, the full power injection indicates an earlier-developed strong concentration of fast ions, but the two achieve the same value later in time. The equalization of signals from the different source rates coincides with the onset of the beam driven instabilities. In this experiment, it is concluded that the core fast H content is limited to $\leq 60\%$ of the TRANSP prediction by fast particle redistribution via beam driven instabilities.

Observation of a beam-driven chirping instability

The previously described beam driven instabilities have been studied well enough to identify nonlinear coupling and fast particle redistribution, and they occur in a plasma with a strong measured velocity gradient (as in Fig. 2). A different flavor of bursting mode is observed when the velocity gradient is mitigated—at lower electron temperature ($T_e(0) \approx 180$ eV, by operating at lower plasma current), the classical slowing of the beam-born ions is reduced to about 10 ms—shorter than the duration of the beam. Figure 9 shows a spectrogram of the $n = 4$ high frequency mode activity. In contrast to the previously discussed beam-driven modes with lifetimes $\leq 100 \mu\text{s}$, the $n = 4$ activity in this discharge also includes several long-lived chirping modes. The frequency whistles down by a factor of two over the comparatively long lifetime of about 1 ms. The fast particle transport associated with this mode is yet to be investigated, and this serves as a reminder that the exploration of fast ion physics in the reversed field pinch configuration is only in its infancy.

SUMMARY

A tangential 1 MW neutral beam injector is enabling studies of the physics of fast ions in the RFP. At low fast particle concentrations, achieved by beam blip experiments, the confinement of fast ions is consistent with classical slowing and transport, even in a stochastic magnetic field. In fact, the

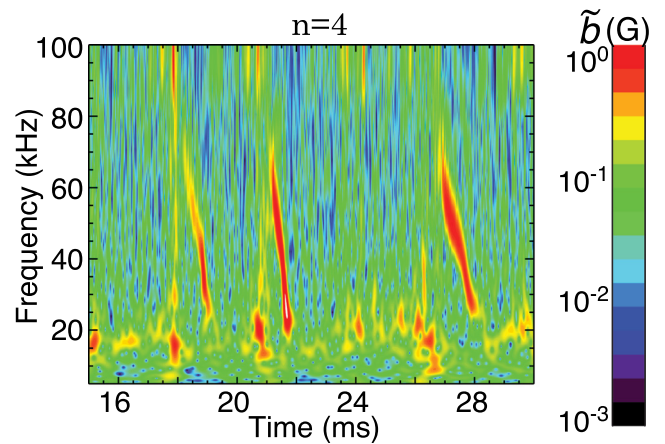


FIG. 9. The $n = 4$ beam driven instability, measured by edge Mirnov coils, exhibits a long-lived distinct chirping feature, where the frequency can drop by more than a factor of two over the course of about 1 ms.

underlying stochasticity has very little effect on the fast ion confinement.

With long (≥ 10 ms) injection periods, the fast ion confinement is sufficient to develop a significant fast ion population. There are several effects on the bulk plasma, including enhanced rotation, electron heating (in the low stochasticity limit), and a change to the current density profile. The stability of the plasma is altered by NBI, in both stabilizing and destabilizing manners, and the effect on the fast ion confinement has been investigated. There is a strong stabilizing influence on the core-most tearing mode and little effect on secondary modes resonant at larger radii. This effect is robust across a wide range of the available equilibria. However, due to a subtle NBI-induced equilibrium change, the up-to 60% reduction of the largest tearing mode does not significantly reduce the core island width or affect the overall stochasticity. As such, there is no observable effect on the fast ion confinement.

In stark contrast, however, the NBI's destabilizing influence has a very strong effect on fast ion confinement. NB injection into standard RFP plasmas with a boundary condition of $q(a) = 0$ leads to simultaneous EPM-like and Alfvénic beam driven instabilities. These modes redistribute core-localized fast ions and lead to a saturation of the core fast ion density. In experiments to date, it is possible to conclude that the actual core fast ion density is less than 60% of the perfectly classical TRANSP prediction. The frequency characteristics and duration of the bursting beam driven instabilities are sensitive to the background plasma conditions, and a long-lived chirping mode is observed with lower core electron temperature. There remain many unexplained observations, and the study of fast ion behavior in the RFP will be rich with physics for the foreseeable future.

ACKNOWLEDGMENTS

The authors wish to acknowledge helpful discussions with B. Heidbrink and N. Crocker, and much assistance from the TRANSP development team at PPPL. This work was supported by USDOE.

- ¹W. W. Heidbrink and G. J. Sadler, *Nucl. Fusion* **34**, 535 (1994).
- ²H. E. Mynick, *Phys. Fluids B* **5**, 1471 (1993).
- ³C. B. Forest, J. R. Ferron, T. Gianakon, R. W. Harvey, W. W. Heidbrink, A. W. Hyatt, R. J. La Haye, M. Murakami, P. A. Politzer, and H. E. St. John, *Phys. Rev. Lett.* **79**, 427 (1997).
- ⁴D. Liu, A. F. Almagri, J. K. Anderson, B. E. Chapman, V. I. Davydenko, P. Deichuli, D. J. Den Hartog, S. Eilerman, G. Fiksel, C. B. Forest, A. A. Ivanov, J. J. Koliner, M. D. Nornberg, S. V. Polosatkin, J. S. Sarff, N. Stupishin, and J. Waksman, in *Proceedings of the 12th IAEA Energetic Particle Meeting*, Austin, Texas 78712, USA, 2011.
- ⁵G. Fiksel, B. Hudson, D. J. Den Hartog, R. M. Magee, R. O'Connell, S. C. Prager, A. D. Beklemishev, V. I. Davydenko, A. A. Ivanov, and Y. A. Tsidulko, *Phys. Rev. Lett.* **95**, 125001 (2005).
- ⁶R. Goldston, D. McCune, H. Towner, S. Davis, R. Hawryluk, and G. Schmidt, *J. Comput. Phys.* **43**, 61 (1981).
- ⁷J. J. Koliner, C. B. Forest, J. S. Sarff, J. K. Anderson, D. Liu, M. D. Nornberg, J. Waksman, L. Lin, D. L. Brower, W. X. Ding, and D. A. Spong, *Phys. Rev. Lett.* **109**, 115003 (2012).
- ⁸L. Lin, W. X. Ding, D. L. Brower, J. J. Koliner, S. Eilerman, J. A. Reusch, J. K. Anderson, M. D. Nornberg, J. S. Sarff, J. Waksman, and D. Liu, *Phys. Plasmas* **20**, 030701 (2013).
- ⁹T. M. Biewer, C. B. Forest, J. K. Anderson, G. Fiksel, B. Hudson, S. C. Prager, J. Sarff, and J. C. Wright, *Phys. Rev. Lett.* **91**, 045004 (2003).
- ¹⁰J. S. Sarff, A. F. Almagri, J. K. Anderson, T. M. Biewer, A. P. Blair, M. Cengher, B. E. Chapman, P. K. Chattopadhyay, D. Craig, D. J. Den Hartog, F. Ebrahimi, G. Fiksel, C. B. Forest, J. A. Goetz, D. Holly, B. Hudson, T. W. Lovell, K. J. McCollam, P. D. Nonn, R. O'Connell, S. P. Oliva, S. C. Prager, J. C. Reardon, M. A. Thomas, M. D. Wyman, D. L. Brower, W. X. Ding, S. D. Terry, M. D. Carter, V. I. Davydenko, A. A. Ivanov, R. W. Harvey, R. I. Pinkster, and C. Xiao, *Nucl. Fusion* **43**, 1684 (2003).
- ¹¹W. F. Bergerson, F. Auriemma, B. E. Chapman, W. X. Ding, P. Zanca, D. L. Brower, P. Innocente, L. Lin, R. Lorenzini, E. Martinez, B. Momo, J. S. Sarff, and D. Terranova, *Phys. Rev. Lett.* **107**, 255001 (2011).
- ¹²R. Lorenzini, E. Martinez, P. Piovesan, D. Terranova, P. Zanca, M. Zuin, A. Alfieri, D. Bonfiglio, F. Bonomo, A. Canton, S. Cappello, L. Carraro, R. Cavazzana, D. F. Escande, A. Fassina, P. Franz, M. Gobbin, P. Innocente, L. Marrelli, R. Pasqualotto, M. E. Puiatti, M. Spolaore, M. Valisa, N. Vianello, and P. Martin, *Nature Phys.* **5**, 570 (2009).
- ¹³R. N. Dexter, D. W. Kerst, T. W. Lovell, S. C. Prager, and J. C. Sprott, *Fusion Technol.* **19**, 131 (1991).
- ¹⁴W. X. Ding, D. L. Brower, B. H. Deng, D. Craig, S. C. Prager, and V. Svidzinski, *Rev. Sci. Instrum.* **75**, 3387 (2004).
- ¹⁵S. Polosatkin *et al.*, "Neutral particle analyzer for studies of fast ion population in plasma," *Nucl. Instrum. Methods Phys. Res. A* (in press).
- ¹⁶S. Eilerman, J. K. Anderson, J. A. Reusch, D. Liu, G. Fiksel, S. Polosatkin, and V. Belykh, *Rev. Sci. Instrum.* **83**, 10D302 (2012).
- ¹⁷J. A. Reusch, J. K. Anderson, V. Belykh, S. Eilerman, D. Liu, G. Fiksel, and S. Polosatkin, *Rev. Sci. Instrum.* **83**, 10D704 (2012).
- ¹⁸W. W. Heidbrink, J. Kim, and R. J. Groebner, *Nucl. Fusion* **28**, 1897 (1988).
- ¹⁹J. Waksman, J. K. Anderson, G. Fiksel, D. Liu, M. D. Nornberg, E. Parke, J. A. Reusch, V. I. Davydenko, P. P. Deichuli, A. A. Ivanov, N. Stupishin, and H. Sakakita, *Phys. Plasmas* **19**, 122505 (2012).
- ²⁰F. Porcelli, *Plasma Phys. Control. Fusion* **33**, 1601 (1991).
- ²¹C. C. Hegna and A. Bhattacharjee, *Phys. Rev. Lett.* **63**, 2056 (1989).
- ²²H. Cai, S. Wang, Y. Xu, J. Cao, and D. Li, *Phys. Rev. Lett.* **106**, 075002 (2011).
- ²³V. A. Svidzinski and S. C. Prager, *Phys. Plasmas* **11**, 980 (2004).
- ²⁴V. V. Mirnov, F. Ebrahimi, C. C. Kim, J. R. King, M. C. Miller, J. A. Reusch, J. S. Sarff, D. D. Schnack, C. R. Sovinec, and T. D. Tharp, in *Proceedings of the 23rd IAEA Fusion Energy Conference*, Daejeon, Republic of Korea, 2010.
- ²⁵A. J. Lichtenberg and M. A. Lieberman, *Regular and Stochastic Motion* (Springer-Verlag, New York, 1983).
- ²⁶A. B. Rechester and M. N. Rosenbluth, *Phys. Rev. Lett.* **40**, 38 (1978).
- ²⁷W. W. Heidbrink, *Phys. Plasmas* **15**, 055501 (2008).
- ²⁸N. A. Crocker, W. A. Peebles, S. Kubota, E. D. Fredrickson, S. M. Kaye, B. P. LeBlanc, and J. E. Menard, *Phys. Rev. Lett.* **97**, 045002 (2006).
- ²⁹M. Podesta, R. E. Bell, N. A. Crocker, E. D. Fredrickson, N. N. Gorelenkov, W. W. Heidbrink, S. Kubota, B. P. LeBlanc, and H. Yuh, *Nucl. Fusion* **51**, 063035 (2011).
- ³⁰E. J. Strait, W. W. Heidbrink, A. D. Turnbull, M. S. Chu, and H. H. Duong, *Nucl. Fusion* **33**, 1849 (1993).